Oxidation kinetics of ZrNbO in steam: differences between the pre-and post-transition stages

Françoise Valdivieso, Marc Tupin, Michèle Pijolat, Michel Soustelle

Oxidation kinetics of ZrNbO in steam: differences between the pre-and post-transition stages

F. Valdivieso[a,*], M. Tupin[b], M. Pijolat[a], M. Soustelle[a]

[a]*Laboratoire des procédés en Milieux Granulaires CNRS UMR 5148, Centre SPIN, Ecole Nationale Supérieure des Mines, 158 Cours Fauriel, 42023 Saint-Etienne, Cedex 2, France, fvaldivieso@emse.fr*
[b]*CEA Saclay, DEN/DMN/SEMI/LM2E, Bâtiment 605, 91191 Gif Sur Yvette Cedex, France, tupin@emse.fr*

Abstract

Zirconium based alloys (and particularly Zircaloy-4) are widely used as cladding material of fuel rods in water-cooled nuclear reactors. However, advanced alloys are now used for longer operation time in more severe conditions. One of these new alloys is a ZrNbO, which contains 1% of Nb as alloying element (instead of Sn in the case of Zircaloy-4).

This ZrNbO alloy, like many zirconium alloys, undergoes a kinetic transition, which is a sharp increase in the oxidation rate when the oxide thickness exceeds a critical value. In the pre-transition stage, the kinetic oxidation curves are approximately parabolic (which is generally interpreted by a diffusion controlling step), and tend towards a quasi-linear behaviour after the transition. Recent studies have shown that the oxygen pressure has an accelerating effect on the oxidation rate of ZrNbO; a platinum layer deposited on the oxide surface has the same effect, both in oxygen and in water vapour. Thus it has been suggested that the oxidation in the pre-transition stage could be described by a mixed reaction-diffusion kinetics. Due to the lack of consistent data on the effect of water vapour on the oxidation rate of ZrNbO before and after the transition, and to confirm (or not) these interpretations, we have studied the oxidation of ZrNbO by isothermal thermogravimetry at 550°C, under controlled partial pressures of water vapour (13 to 80 hPa) and hydrogen (10 hPa). The aim is to verify if the oxidation proceeds in a steady state and if there is a rate-limiting step in one (or both) stages, and to clearly evidence the differences between the pre- and post transition stages from the kinetic point of view.

TG-DSC experiments have shown that the system is in a steady state from the beginning of the oxidation, in the pre- and post-transition stages. Then, the existence of a rate-limiting step was verified using an experimental method based on temperature or pressure jumps: it has been concluded that this assumption is valid in both stages, which is not compatible with the assumption of a mixed reaction-diffusion controlled rate).

Moreover, it comes out that the kinetic behaviour is different before and after the transition: the influence of temperature jumps is greater in pre-transition, whereas the effect of water vapour partial pressure is more pronounced in post-transition (nevertheless, an accelerating effect is also observed before the transition). No influence of hydrogen partial pressure has been observed. Besides, the higher the Nb content in the alloy, the higher the oxidation rate (in pre-transition). A mechanism has been proposed to account for the results obtained in pre-transition, involving the diffusion of adsorbed species in the porous part of the oxide layer as rate-determining step.

Keywords**:** ZrNbO ; oxidation ; kinetics ; water vapour ; steady state ; rate-limiting step.

Introduction

Despite numerous works dedicated to the oxidation kinetics of zirconium alloys by pressurized water, water vapour or oxygen, the mechanisms and the rate-limiting steps for zirconia growth are not already established. It is well known that after a pseudo-parabolic first period [1-3], a kinetic transition occurs when the thickness of the oxide layer exceeds a critical value, which corresponds to an increase in the oxidation rate, associated with the appearance of cracks and pores in the oxide layer [2, 4, 5]. In the post-transition stage, the oxidation curves are considered to be either linear [4] or to result from cyclic periods of increasing and decreasing rate [6].

In a previous work dedicated to the oxidation of Zircaloy-4 by water vapour [7], we have shown that great differences exist between the pre and post-transition stages, from the kinetic point of view: before the transition, the oxidation rate is controlled by the diffusion of oxygen vacancies in the oxide layer, as usually suggested in the literature data, whereas in the post-transition stage, the assumption of the rate-limiting step is no more valid.

As far as the oxidation of Nb-containing alloys is concerned, the shape of the kinetic curves (weight gain versus time) is qualitatively similar to that obtained with zircaloys. Nevertheless, Nb-containing alloys are oxidised faster than recrystallised Zircaloy in oxygen and in water vapour [4, 8-12], at the beginning of the oxidation, but the kinetic transition is not so sharp in Nb-containing alloys and it occurs after a longer time. In autoclave, different results are obtained, these alloys showing in most cases a better resistance to corrosion [14, 15].

Another difference between the two alloys is related to the effect of platinum on the oxidation rate: if platinum is deposited on the surface of an oxide layer grown on ZrNbO, in pre-transition, the oxidation rate increases, in oxygen [10] or in water vapour [11], whereas Pt has no effect on the oxidation of Zy4 [11, 12].

Moreover, it has been shown that the oxidation rate depends on the niobium concentration in the zirconium alloy [16], and on the oxygen pressure [17].

In order to account for these results, the pre-transition stage of the oxidation of ZrNbO is suggested to be controlled by a mixed diffusion-reaction regime, and therefore in steady conditions [10, 13].

Finally, due to the lack of consistent data on the effect of water vapour on the oxidation rate before and after the transition, and in order to confirm (or not) these interpretations, we have studied the oxidation of a Nb-containing zirconium alloy, ZrNbO alloy, at 530°C, following the same methodology as in the case of Zircaloy-4 [7]. This approach is principally based on the verification of kinetic assumptions that are usually made *a priori*. The oxide scale growth is assumed to be described by a series of elementary steps, one of them being rate-determining. This assumption implies that (i) the system is in a steady state and (ii) the oxidation rate can be written as:

$$\frac{d\alpha}{dt} = \Phi\left(T, P_i\right).E(t) \qquad (1)$$

in which α is the fractional conversion, Φ is a rate per unit area ($mol.s^{-1}.m^{-2}$), it depends on the nature of the rate-limiting step (diffusion, interface reaction), it is independent on time but may be a function of temperature T and partial pressures of the gases P_i. E(t) ($m^2.mol^{-1}$) is a function related to the extent of the reaction zone where the rate-limiting step is located.

In this paper, the assumptions (i) and (ii) will be verified experimentally, then the variations of Φ with P_{H2O} and P_{H2} will be obtained, using a method based on pressure jumps. These results will allow to clearly identify the differences between the pre and post-transition stages, and a mechanism will be proposed for the pre-transition.

Experimental results

Experimental. A 0.4 mm thick sheet of recrystallised ZrNbO alloy was used, and samples were cut to 10 x 10 mm for thermogravimetric experiments, and 15 x 15 mm for simultaneous thermogravimetry and calorimetry experiments. The alloy composition is indicated in *Table I.* The sample surface was cleaned with an equimolar solution of ethanol and acetone in ultrasonic waves, then with pure ethanol and dried with compressed air.

Fe (ppm)	O (ppm)	Nb (%)
354	1303	1.03

Table I : Composition of the ZrNbO alloy

The oxidation curves were obtained in isothermal and isobaric conditions at 500 and 530°C with a symmetrical thermoanalyser SETARAM TAG16, under a flowing mixture of water vapour and hydrogen in helium. The flowrate of the gases was controlled by mass-flowmeters (Brooks 5850S), the total flowrate being 2.3 $l.h^{-1}$, and the partial pressure of hydrogen being usually equal to 10 hPa. The water vapour partial pressure was fixed in the range 13-80 hPa, using thermoregulated baths. It was controlled using humidity sensors (Transmicor 241-242 Coreci), placed at the inlet and outlet of the thermobalance furnace.

Jumps in hydrogen pressure were carried out by changing the flowmeter setpoint, whereas jumps in water vapour pressure were performed by switching the gaseous flow from one water bath to another one maintained at a different temperature.

The simultaneous thermogravimetry and calorimetry experiments were performed using a Setaram TG/DSC 111, under flowing mixtures of water vapour and hydrogen in helium.

The morphology of the oxide layers was observed by scanning electron microscopy (SEM DSM 960A Zeiss).

Shape of the kinetic curves. *Fig. 1* represents a kinetic curve giving the mass gain per unit area m/S(t) versus time, and its derivative ($d(m/S)/dt$), obtained at 530°C (after an initial temperature rise of 30°C/min from room temperature to 530°C), under 10 hPa in hydrogen and 13 hPa in water vapour. The minimum of the rate corresponds to an oxide thickness (calculated from the weight gain) of about 10 µm. The curve appears to be approximately parabolic in the pre-transition stage, whereas the rate is constant after the transition.

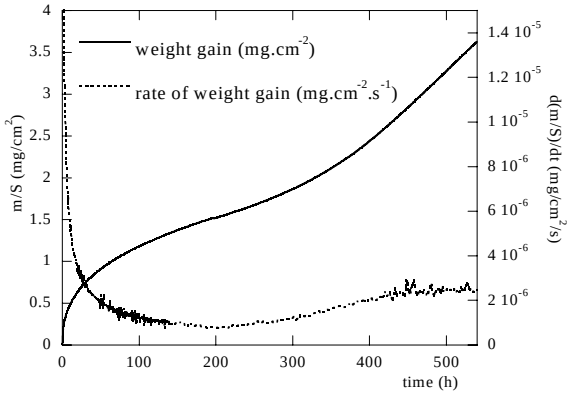

Fig. 1 : Weight gain (—) and its derivative (---) versus time for ZrNbO at 530°C in water vapour (13 hPa) and hydrogen (10 hPa), showing the pre- and post-transition stages.

Steady state approximation. In *Fig. 2*, the variations of the rate of weight gain (dm/dt) and the heat flow dQ/dt versus time are represented in the pre-transition stage, at 550°C. A scaling factor allowing to superimpose the two curves could be found, which shows that the reacting system is in a steady state before the transition.

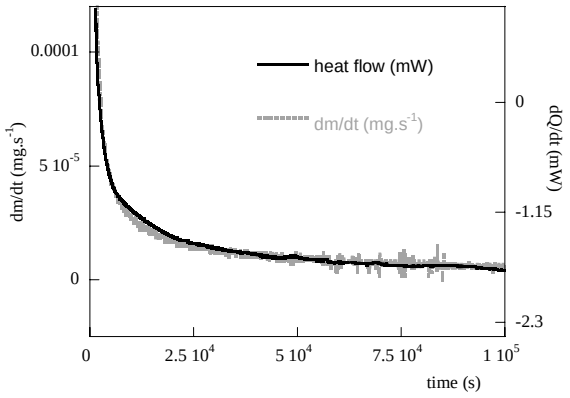

Fig. 2 : Rate of weight gain (--- dm/dt) and heat flow (—) versus time for ZrNbO at 550°C in water vapour (13 hPa) and hydrogen (10 hPa), for the pre-transition stage.

Several experiments were performed up to the transition, confirming the results of *Fig. 2*. Unfortunately, only the very beginning of the transition was reached in TG/DSC experiments, the linear regime characteristic of the post-transition stage could not be reached, even for experiments lasting more than one month. Consequently, the steady state approximation could not be verified after the transition.

Rate-determining step assumption. When a rate-limiting step can be assumed, Eq. (1) gives the variations of the oxidation rate with the intensive variables (T, P_i…) and the time. In isobaric and isothermal conditions, $\Phi(T,P_i)$ is constant, then a sudden change (jump) in temperature or partial pressure during an experiment will then lead to a change in Φ, while E(t) will remain approximately constant (provided that the time necessary for the T or P change is short enough).

Thus the ratio of the rates measured after (at the right side) and before (at the left side) the jump is equal to Φ_r / Φ_l (E(t) being eliminated in the ratio). Performing a series of similar jumps at various reaction times will lead to a series of Φ_r / Φ_l ratios, which must be identical if Eq. (1) can be applied.

This method, that we have named the "ΦE test", has been successfully used in previous works [7, 17-22]. The results are indicated on *Fig. 3*, for sudden changes in temperature from 500 to 530°C (P_{H_2O} = 13 hPa, P_{H_2} = 10 hPa) in pre-transition stage (*Fig. 3a*), and from 530 to 500°C in post-transition (*Fig. 3b*).

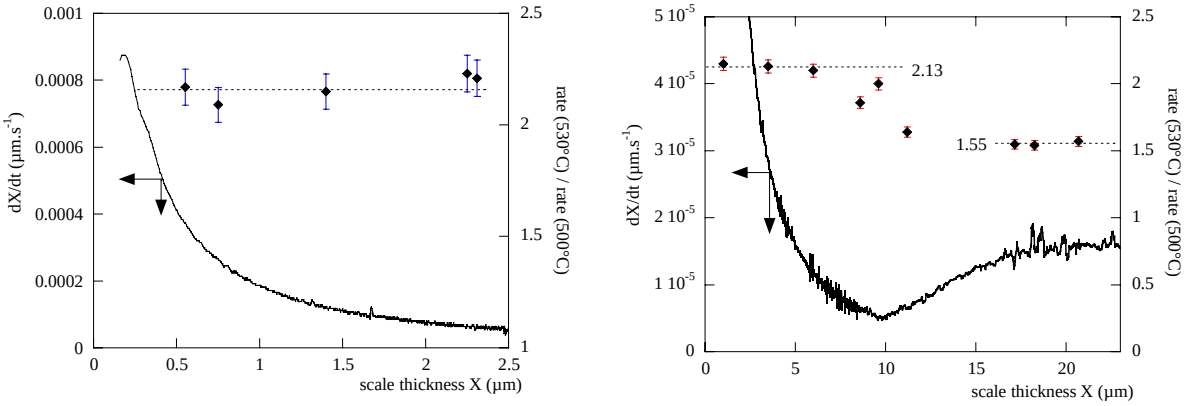

(a) (b)

Fig. 3 : Rate of weight gain (530°C, P_{H2O} = 13 hPa, P_{H2} = 10 hPa) and ratios of the rate before and after the temperature jumps, in the pre- (a) and post-transition (b) stages.

Considering the experimental errors bars, the ratio keeps a constant value (2.17 ± 0.1 for temperature jumps from 500 to 530°C (*Fig. 3a*) and 2.13 ± 0.1 for temperature jumps from 530 to 500°C (*Fig. 3b*)) during the pre-transition stage, up to about 6 µm. Then the ratio decreases between 6 µm and 12 µm, during the transition, and becomes again constant after 17 µm, in the post-transition stage (characterized by a linear regime with a constant rate).

Consequently, it can be concluded that the "ΦE test" is validated in the pre-transition domain; as the steady state assumption is also verified, there exists a rate-limiting step in this stage (moreover, a mixed diffusion-reaction controlling rate is not in agreement with the results of the "ΦE test", because in such a case the ratios of the rates would not be constant [11, 20]). The "ΦE test" is also verified in the post-transition stage, but the value of the ratio is clearly lower than its value in the pre transition stage (1.55 ± 0.08 instead of 2.13 ± 0.1). Obviously, a change in the rate-limiting step occurs between the pre and post-transition stages, since the shape of the curves and the values of the rate ratios are different.

Effect of H_2O and H_2 partial pressures. The variations of Φ with a gas partial pressure P can easily be obtained by performing sudden changes, from P_0 to P, at a given thickness X, the ratio of the rates being then equal to $\Phi(P)/\Phi(P_0)$ [7, 17, 19, 21]. The experiments were carried out at 500°C, with 10 hPa in hydrogen and a water vapour pressure varying from 13 hPa (P_0) to 80 hPa after the jump. For the hydrogen pressure jumps, the water pressure was fixed at 13 hPa and the hydrogen pressures changed from 10 hPa (P_0) to 40 hPa.

The variations of Φ with P_{H_2O} in pre-transition are represented on *Fig. 4a:* the water vapour pressure has a slight accelerating effect. In the post-transition stage, jumps in water vapour pressure have been performed at an oxide thickness equal to 25 µm (in the linear part of the curves), from 13 hPa to 80 hPa: the Φ function increases with P_{H_2O}, the accelerating effect being more pronounced than in the pre-transition stage (*Fig. 4b*). On the contrary, the hydrogen pressure has no effect on the oxidation rate [22].

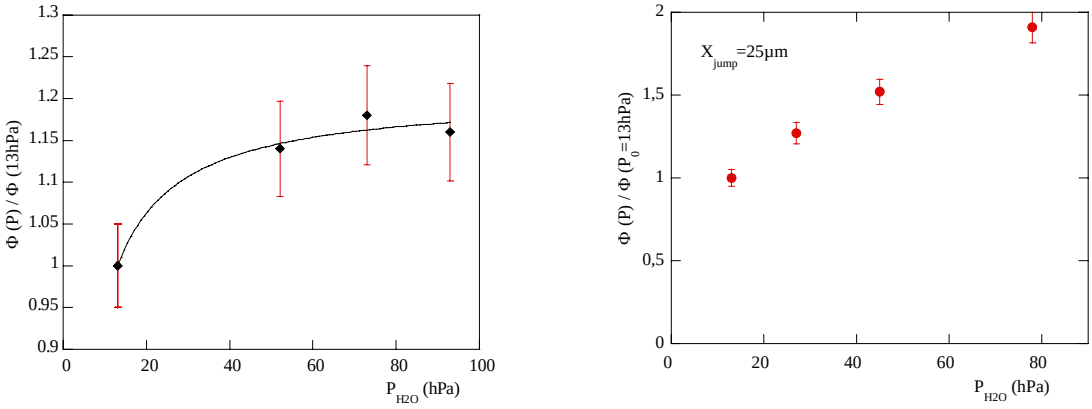

(a) (b)

Fig. 4 : Variations of the reactivity of growth Φ with the partial pressure of water vapour, (a) in the pre-transition stage (jumps from P_{H2O} = 13 hPa to P, for X = 2.5µm, T = 500°C, P_{H2} = 10 hPa), (b) in post-transition (jumps from P_{H2O} = 13 hPa to P, for X = 25µm, T = 530°C, P_{H2} = 10 hPa).

Effect of Nb content. An alloy containing 0.4%wt in niobium (Zr0.4%NbO) has been used, in order to compare its oxidation behaviour to ZrNbO one. This alloy does not contain β-Nb precipitates but contains $Zr(Nb, Fe)_2$ phases [23]. The oxidation curves giving the oxide thickness X versus time, obtained for the two alloys at 520°C under 13 hPa in hydrogen and 67 hPa in water vapour are represented on *Fig. 5a*. It can be seen that the higher the Nb

content, the higher the oxidation rate in pre-transition (which is in agreement with the literature data) [16, 24-26]. The post-transition stage was not reached, in the experiment, with Zr0.4%NbO alloy.

Fig. 5b shows the rate curves dX/dt versus X for both alloys. As a scaling factor allowing to superimpose the two curves could be found, the oxidation rates of these two alloys remain proportional during all the reaction time, with a ratio equal to 1.5 (which is lower than the ratio of the Nb concentration in the alloys (equal to 2.5)).

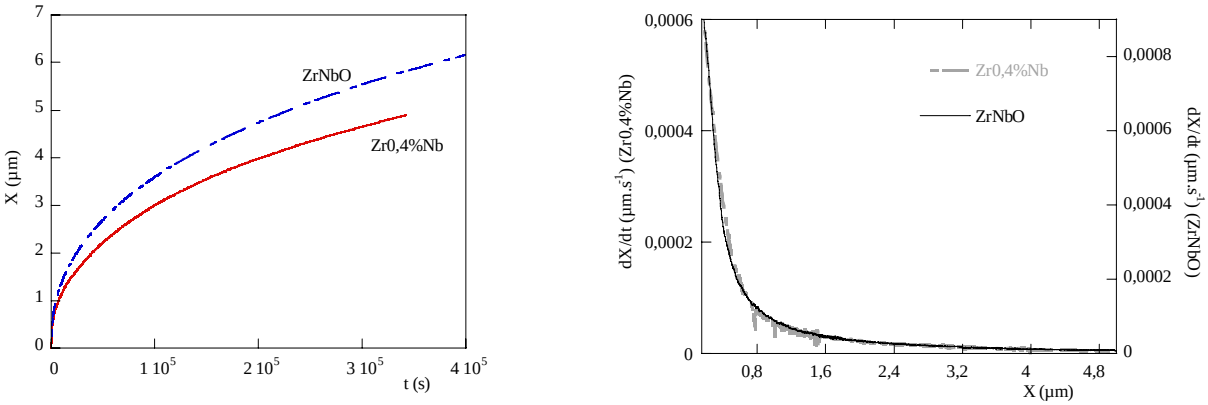

(a) (b)

Fig. 5 : (a) Oxide thickness versus time for ZrNbO and Zr0.4%Nb (T = 520°C, P_{H2O} = 13hPa, P_{H2} = 10 hPa), and (b) oxidation rate (dX/dt) versus time for Zr0.4%Nb (—) and ZrNbO (---).

Characterisation of the samples. The cross sectional views of the oxide scale grown during the pre-transition stage present a continuous and uniform layer adherent to the substrate. *Fig. 6* shows micrographs of samples oxidised at 530°C in 13 hPa and 10 hPa of water vapour and hydrogen respectively. The thickness calculated from the weight gain is 3.5 µm for *Fig. 6a* and 6 µm for *Fig. 6b*. The metal/oxide interface is more or less undulated, and short cracks parallel to the interface appear regularly inside the layer [9]. A delayed oxidation can also be observed straight above some of these cracks.

Similar cracks are observed in samples oxidised after the kinetic transition, up to an oxide thickness of 12 µm and more. Moreover, new large cracks are observed which are perpendicular to the metal/oxide interface and connected to the gaseous atmosphere.

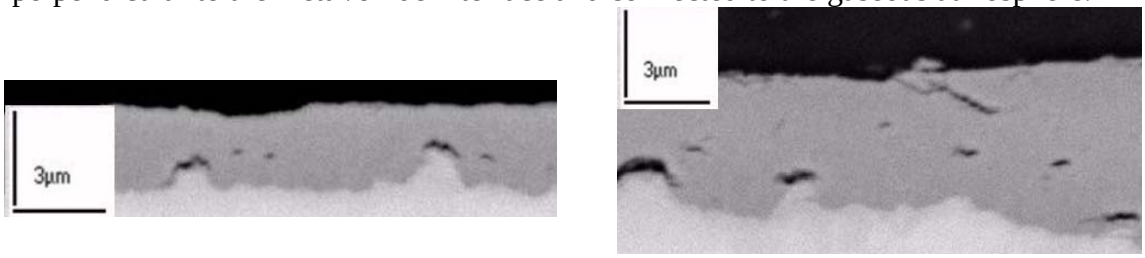

(a) (b)

Fig. 6 : Cross-sectional views of oxide layers grown on ZrNbO at 530°C (P_{H2O} = 13 hPa, P_{H2} = 10 hPa) : X ≈3.5 µm (a) and X ≈6 µm (b).

Discussion.

Pre-transition. Since the steady-state and the "ΦE test" have been validated experimentally, the assumption of a rate determining step can be made and the oxidation rate is given by (X is the oxide thickness):

$$\frac{dX}{dt} = \frac{V_{ox} n_o}{2S_o} \Phi(T, P_i)\, E(t) \qquad (2)$$

where V_{ox} is the molar volume of the oxide ($m^3.mol^{-1}$), n_0 is the initial amount of metal (mol), S_0 is the surface of the samples (m^2).

It has been observed that the Φ function increases with the partial pressure of water vapour. A simple mechanism involving oxygen vacancies can be written to describe zirconia growth [7], which provides a good interpretation of the oxidation of Zircaloy-4. From this mechanism, it is well-known that only a rate-limiting step located at the external interface (gas/oxide) can account for an accelerating effect of the partial pressure on the Φ function [7].

If such an interface step was rate-limiting, the oxidation rate should be constant with time and the kinetic curves should be linear, which is not the case. Some authors [10, 13] have interpreted the curves with a mixed reaction-diffusion rate, but this assumption is not in agreement with our experimental results [20, 22].

Consequently, a new mechanism has to be proposed to describe zirconia growth on ZrNbO alloy. The dissociation of water vapour at the surface of the oxide probably leads to the formation of adsorbed hydroxyl groups (OH) and then, the diffusion of such species through the oxide layer may predominate. Considering the SEM micrographs of our samples (*Fig.6*), the oxide layer appears to be homogeneous (excepted a few cracks). Nevertheless, it has been found by impedance spectroscopy [10, 27] that the oxide layer grown on ZrNbO could be divided into two sub-layers. For the kinetic modelling, two possibilities can be imagined, involving one or two oxide layers:

- either one oxide layer with micropores and diffusion of adsorbed species via this porosity,
- or two oxide layers: the microporous layer and a very thin and dense layer near the metal/oxide interface (for example, the native oxide layer), in which the diffusion of oxygen vacancies is very rapid. The thickness of this dense layer is assumed to remain very small during all the pre-transition stage.

In both cases, the weight gain is considered to be due only to the growth of the microporous oxide layer. The oxygen transport through this layer is supposed to occur via adsorbed hydroxyl groups (as seen in the mechanism below) ; thus, a part of the hydrogen produced by the oxidation is released near the metal/oxide interface. Adsorbed hydrogen can migrate through the micropores towards the external interface.

The various steps involved in the growth mechanism are detailed in *Table II*.

Interfaces	Elementary steps	
External interface	(1) adsorption of water on adsorption sites s:	$H_2O + s \underset{\leftarrow}{\overset{\rightarrow}{}} H_2O - s$
	(2) dissociation of water into OH groups:	$H_2O - s + s \underset{\leftarrow}{\overset{\rightarrow}{}} OH - s + H - s$
	(3) reduction of hydroxyl groups:	$OH - s + e' \underset{\leftarrow}{\overset{\rightarrow}{}} OH^- - s$
	(4) desorption of hydrogen:	$2H - s \underset{\leftarrow}{\overset{\rightarrow}{}} H_2 + 2s$
	(5) diffusion of adsorbed OH^- groups in the porous layer.	
Intermediate interface (porous layer/ dense layer) :	(6) interface step :	$OH^- - s + V_O^{\bullet\bullet} + e' \underset{\leftarrow}{\overset{\rightarrow}{}} H - s + O_O$
	(7) H_2 desorption at the intermediate interface :	$2H - s \underset{\leftarrow}{\overset{\rightarrow}{}} H_2 + 2s$
	(8) diffusion of oxygen in the dense layer.	
Internal interface :	(9) internal interface step:	$Zr_{alloy} \underset{\leftarrow}{\overset{\rightarrow}{}} Zr_{Zr_{(OX)}} + 2V_O^{\bullet\bullet} + 4e'$

Table II: Oxide growth mechanism in pre-transition.

The hydrogen amount in the metal can be neglected in the total weight gain (this is in agreement with the very low amount of hydrogen measured by Cezus in the metal in the pre-transition stage (about 30 ppm)).

In order to account for the decrease in the rate versus time in pre-transition, we have to consider a diffusion step as rate-limiting. The kinetic curves being not strictly parabolic, we have successfully fitted them using the following equation (as previously done in our study of Zircaloy-4 oxidation [7]):

$$\frac{dX}{dt} = \frac{k_1}{X}\exp(-k_2 X) \qquad (3)$$

in which X represents the thickness of the microporous layer.

The curves giving the rate dX/dt versus X were fitted using several laws (parabolic, cubic, power…), the comparison of these fits are given in *Fig. 7*. Eq. (3) always leads to the best agreement with all our experiments.

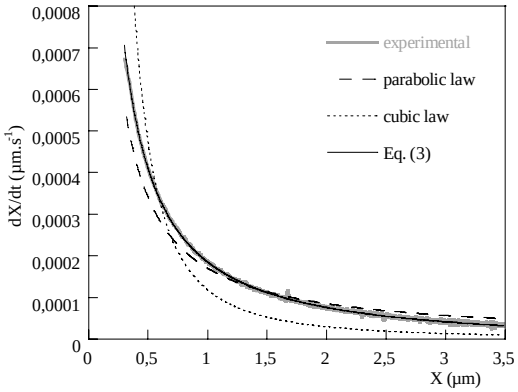

Fig.7 : Rate of oxidation of ZrNbO as a function of the oxide thickness before the kinetic transition – comparison with various rate laws.

From Eq. (3), by comparison to Eq. (2), the $\Phi(T,P_i)$ and E(t) functions can be easily calculated [22]:

$$\Phi(T,P_i) = \frac{D \,.\, C}{X_O} \quad \text{and} \quad E(t) = \frac{D.C\,S_0 X_0}{n_0}\frac{\exp(-k_2 X)}{X} \qquad (4)$$

X_0 is a characteristic length, for example the initial thickness of the sample. The variations with temperature and partial pressures of the $\Phi(T,P_i)$ function are deduced from the growth mechanism detailed above. Assuming that the rate-limiting step is the diffusion of adsorbed hydroxyl groups $OH^{\cdot}$-s from the external interface into the porous layer via the surface of the pores, and neglecting the concentration of $OH^{\cdot}$-s groups at the interface of arrival, the Φ function can be calculated :

$$\Phi(T,P_i) = \frac{D}{X_0}\theta_0 \frac{K_1 K_2 K_3 \beta P_{H_2O}}{P_{H_2O}\left(K_1 K_2 (1 + K_3\beta) + K_1\sqrt{\frac{P_{H_2}}{K_4}}\right) + \sqrt{\frac{P_{H_2}}{K_4}} + \frac{P_{H_2}}{K_4}} \qquad (5)$$

in which K_i is the equilibrium constant of the step (i), θ_0 is the concentration of adsorption sites per unit of surface area, and β is the electrons activity in the oxide layer, which is supposed to be fixed by the Nb content in solid solution in the oxide ($[e'] = [Nb_{Zr}^{\bullet}] = \beta$).

The variations of $\Phi(T,P_i)$ with P_{H_2O} follow an hyperbolic law, which is in a good agreement with the experimental data, as shown in *Fig. 4a* (continuous line).

From Eq. (5), $\Phi(P)$ should vary with hydrogen pressure like $\frac{1}{a + b\,P_{H_2} + c\sqrt{P_{H_2}}}$, but no influence of P_{H_2} was observed experimentally in the range (2.5 - 40hPa). However, this law exhibits a constant behaviour when P_{H2} increases, so experiments at lower hydrogen pressure would have been useful to validate it. Besides, Eq.(5) shows that if the value of the equilibrium constant K_4 is high compared to the values of P_{H2}, the term $\frac{P_{H_2}}{K_4}$ may become very small and may be neglected besides the other terms. In that case, no effect of hydrogen

pressure would be observed on the oxidation rate. Unfortunately, information on the values of the various equilibrium constants are not available in order to support one of these suggestions.

Moreover, the $\Phi(T,P_i)$ function increases when the Nb content in solid solution in the oxide, β, increases, which is in agreement with our experimental results [22].

It has also been observed that platinum has an accelerating effect on the oxidation rate of ZrNbO [10, 11], in water vapour or oxygen. As the platinum layer leads to an increase of the equilibrium constant K_3 [22], this model allows to propose an interpretation of the effect of platinum on the oxidation rate of ZrNbO.

Finally, we have shown that the pre-transition stage in ZrNbO oxidation cannot be accounted for by the mechanism usually proposed for the oxidation of zirconium alloys, which involves the diffusion of oxygen vacancies through the dense oxide layer as the rate controlling step. Thus, we have proposed another mechanism allowing to account for the accelerating effect of water vapour and Nb content. The important feature is to demonstrate that it is possible to explain the influence of the gases without assuming necessarily an interface rate-limiting step. In the case of ZrNbO, the oxidation is assumed to be controlled by a diffusion step, in which the concentration gradient of the diffusing species is fixed by a step located at the external interface (and not by a step located at the metal/oxide interface, as in the mechanism proposed usually).

Transition and post-transition. It is clear from the results of the jumps method (*Fig. 3b* and *4*) that the diffusion step controlling the beginning of the oxidation is no longer valid, even before the rate reaches its lowest value (since the ratios of the rates obtained with the jumps method decreases from about 7 µm, whereas the oxidation rate is minimum at about 10 µm, see *Fig. 3b*). Large cracks connecting a part of the oxide layer to the gaseous atmosphere appear from this point, which could be related to the increase in the rate after the transition.

Then, when the oxide thickness exceeds 17 µm, the shape of the kinetic curve is linear. Moreover, the ratio of the rates remains constant (with a value different from the pre-transition one, see *Fig. 3b*). Consequently, it can be deduced that the post-transition stage is controlled by an interface step, largely influenced by the water vapour pressure. Another possibility could be the diffusion through a layer with a constant thickness, but this is less probable due to the influence of the water vapour pressure.

The pre-transition mechanism could explain the post-transition kinetics if the rate of one of the interface steps of this mechanism became far lower in post-transition than it was in pre-transition [22]. Another way to explain the post-transition kinetics would be a change in the mechanism, involving completely different steps. Unfortunately, we have no experimental evidence to support one of these suggestions. More investigations would be necessary to give a valuable interpretation of the post-transition kinetics.

Conclusions

The oxidation of a ZrNbO alloy in a mixture of hydrogen and water vapour at 530°C exhibits clear differences between the pre- and post-transition stages.

In pre-transition, the oxidation proceeds in a steady state, and is influenced by water vapour and Nb content, whereas hydrogen pressure has no effect in the studied range. The rate decreases with time, according to a sub-parabolic law.

A mechanism has been proposed to account for these results, which involves the diffusion of adsorbed OH groups in a microporous part of the oxide layer, as rate-determining step.

Then, after a transition period beginning at about 7 µm at 530°C, a rate limiting step can again be considered when the oxide thickness is higher than 17 µm. As the curves are linear,

the oxidation is probably controlled by an interface step. This step has not been determined, but it is probably different from the steps proposed in the pre-transition mechanism.

Consequently, the transition is accompanied by a change in the oxidation mechanism, that could be linked to the change in the morphology of the oxide layer.

Acknowledgements
This work has been carried out with the financial support of FRAMATOME-ANP. We would like thank P. Barberis (Cezus) and A. Frichet (Framatome-ANP) for helpful discussions.

References
1. H.A. Porte, J.G. Schnizlein, R.C. Vogel, D.F. Fisher, *J. Electrochem. Soc.*, **107** (1960) 506.
2. J.K. Dawson, G. Long, W.E. Seddon, J.F. White, *J. Nucl. Mater.,* **25** (1968) 179.
3. T. Arima, K. Moriyam, N. Gaja, H. Furuya, K. Idemitsu, Y. Inagaki, *J. Nucl. Mater.,* **257** (1998) 67.
4. B. Cox, *J. Nucl. Mater.,* **148** (1987) 332.
5. J.J. Kearns, *J. Nucl. Mater.,* **22** (1967) 292.
6. M. Parise, thesis, Paris, 1996.
7. M. Tupin, M. Pijolat, F. Valdivieso, M. Soustelle, A. Frichet, P. Barberis, *J. Nucl. Mater.,* **317** (2003) 130.
8. N. Petigny, P. Barberis, C. Lemaignan, C. Valot, M. Lallemant, *J. Nucl. Mater.,* **280** (2000) 318.
9. P. Bossis, thesis, Grenoble, 1999.
10. J.J. Vermoyal, A. Frichet, L. Dessemond, *J. Nucl. Mater.,* **328** (2004) 31.
11. M. Tupin, thesis, Saint-Etienne, 2002.
12. J.J. Vermoyal, L. Dessemond, A. Hammou, A. Frichet, *J. Nucl. Mater.,* **298** (2001) 297.
13. A. Frichet, P. Barberis, N. Petigny, in: 12th Symposium on Zirconium in the Nuclear Industry, Toronto, 15-18 June 1998.
14. G.P. Sabol, G.R. Kilp, M.G. Balfour, E. Roberts, Zirconium in the Nuclear Industry, 8th International Symposium, *ASTM STP* **1023** (1989) 227.
15. J.P. Mardon, D. Charquet, J. Senevat, *Proceedings of the International Meeting on Light Water Reactor Fuel Performance*, West Pam Beach, Florida, April 17-21, (1994) 643.
16. K.N. Choo, S. Pyun, Y. Kim, *J. Nucl. Mater.,* **226** (1995) 9.
17. M. Tupin, M. Pijolat, F. Valdivieso, M. Soustelle, A. Frichet, P. Barberis, *Mater. Sci. Forum*, Trans Tech Publications, Switzerland, **461-464** (1) (2004) 13.
18. K. Surla, F. Valdivieso, M. Pijolat, M. Soustelle, M. Prin, *Ann. Chim. Sci. Mater.,* **25** (2000) 601.
19. K. Surla, F. Valdivieso, M. Pijolat, M. Soustelle, M. Prin, *Solid State Ionics,* **143** (2001) 355.
20. F. Ledoux, F. Valdivieso, M. Pijolat, M. Soustelle, A. Frichet, P. Barberis, *Mater. Sci. Forum*, Trans Tech Publications, Switzerland**, 369-372** (1) (2001) 223.
21. K. Nahdi, S. Perrin, M. Pijolat,F. Rouquerol, N. Ariguib, M. Ayadi, *Phys. Chem. Chem. Phys.*, **4** (2002) 1972.
22. M. Tupin, M. Pijolat, F. Valdivieso, M. Soustelle, *J. Nucl. Mater.,* in press.
23. P. Barberis, D. Charquet, V. Rebeyrolle, *J. Nucl. Mater.,* **326** (2004) 163.
24. H.H. Klepfer, *J. Nucl. Mater.,* **9** (1963) 65.
25. Y.H. Jeong, H.G. Kim, D.J. Kim, B.K. Choi, J.H. Kim, *J. Nucl. Mater.,* **323** (2003) 72.
26. H.G. Kim, Y.H. Jeong, T.H. Kim, *J. Nucl. Mater.,* **326** (2004) 125.
27. F. Garzarolli, H. Seidel, R. Tricot, J.P. Gros, Zirconium in the Nuclear Industry, 9th International Symposium, *ASTM STP* **1132** (1991) 395.